Magnetic-Field-Induced Kondo Effects in Coulomb Blockade Systems

M. Pustilnik[1], L. I. Glazman[1], D. H. Cobden[2], and L. P. Kouwenhoven[3]

[1] Theoretical Physics Institute, University of Minnesota, 116 Church St. SE, Minneapolis, MN 55455, USA
[2] Department of Physics, University of Warwick, Coventry, CV4 7AL, UK
[3] Department of Applied Physics and ERATO Mesoscopic Correlation Project, Delft University of Technology, P. O. Box 5046, 2600 GA Delft, the Netherlands

Abstract. We review the peculiarities of transport through a quantum dot caused by the spin transition in its ground state. Such transitions can be induced by a magnetic field. Tunneling of electrons between the dot and leads mixes the states belonging to the ground state manifold of the dot. Unlike the conventional Kondo effect, this mixing, which occurs only at the singlet-triplet transition point, involves both the orbital and spin degrees of freedom of the electrons. We present theoretical and experimental results that demonstrate the enhancement of the conductance through the dot at the transition point.

1 Introduction

Quantum dot devices provide a well–controlled object for studying quantum many-body physics. In many respects, such a device resembles an atom imbedded into a Fermi sea of itinerant electrons. These electrons are provided by the leads attached to the dot. The orbital mixing in the case of quantum dot corresponds to the electron tunneling through the junctions connecting the dot with leads. Voltage V_g applied to a gate – an electrode coupled to the dot capacitively – allows one to control the number of electons N on the dot. Almost at any gate voltage an electron must have a finite energy in order to overcome the on-dot Coulomb repulsion and tunnel into the dot. Therefore, the conductance of the device is suppressed at low temperatures (Coulomb blockade phenomenon[1]). The exceptions are the points of charge degeneracy. At these points, two charge states of the dot have the same energy, and an electron can hop on and off the dot without paying an energy penalty. This results in a periodic peak structure in the dependence of the conductance G on V_g. Away from the peaks, in the Coulomb blockade valleys, the charge fluctuations are negligible, and the number of electrons N is integer.

Every time N is tuned to an odd integer, the dot must carry a half-integer spin. In the simplest case, the spin is $S = 1/2$, and is due to a single electron residing on the last occupied discrete level of the dot. Thus, the quantum dot behaves as $S = 1/2$ magnetic impurity imbedded into a tunneling barrier between two massive conductors. It is known[2] since mid-60's that the presence of such impurities leads to zero-bias anomalies in tunneling conductance[3], which are

R. Haug and H. Schoeller (Eds.): LNP 579, pp. 3–24, 2001.
© Springer-Verlag Berlin Heidelberg 2001

adequately explained[4] in the context of the Kondo effect[5]. The advantage of the new experiments[6] is in full control over the "magnetic impurity" responsible for the effect. For example, by varying the gate voltage, N can be changed. Kondo effect results in the increased low–temperature conductance only in the odd–N valleys. The even–N valleys nominally correspond to the $S = 0$ spin state (non-magnetic impurity), and the conductance decreases with lowering the temperature.

Unlike the real atoms, the energy separation between the discrete states in a quantum dot is fairly small. Therefore, the $S = 0$ state of a dot with even number of electrons is much less robust than the corresponding ground state of a real atom. Application of a magnetic field in a few–Tesla range may result in a transition to a higher-spin state. In such a transition, one of the electrons residing on the last doubly–occupied level is promoted to the next (empty) orbital state. The increase in the orbital energy accompanying the transition is compensated by the decrease of Zeeman and exchange energies. At the transition point, the ground state of the dot is degenerate. Electron tunneling between the dot and leads results in mixing of the components of the ground state. Remarkably, the mixing involves spin as well as orbital degrees of freedom. In this paper we demonstrate that the mixing yields an enhancement of the low–temperature conductance through the dot. This enhancement can be viewed as the magnetic–field–induced Kondo effect.

We present the model and theory of electron transport in the conditions of the field-induced Kondo effect in Section 2. The experimental manifestations of the transition observed on GaAs vertical quantum dots and carbon nanotubes are described in Section 3.

2 The Model

We will be considering a confined electron system which does not have special symmetries, and therefore the single-particle levels in it are non-degenerate. In addition, we assume the electron-electron interaction to be relatively weak (the gas parameter $r_s \lesssim 1$). Therefore, discussing the ground state, we concentrate on the transitions which involve only the lowest-spin states. In the case of even number of electrons, these are states with $S = 0$ or $S = 1$. At a sufficiently large level spacing $\delta \equiv \epsilon_{+1} - \epsilon_{-1}$ between the last occupied (-1) and the first empty orbital level $(+1)$, the ground state is a singlet at $B = 0$. Finite magnetic field affects the orbital energies; if it reduces the difference between the energies of the said orbital levels, a transition to a state with $S = 1$ may occur, see Fig. 1. Such a transition involves rearrangement of two electrons between the levels $n = \pm 1$. Out of the six states involved, three belong to a triplet $S = 1$, and three others are singlets $(S = 0)$. The degeneracy of the triplet states is removed only by Zeeman energy. The singlet states, in general, are not degenerate with each other. To describe the transition between a singlet and the triplet in the ground

state, it is sufficient to consider the following Hamiltonian:

$$H_{\rm dot} = \sum_{ns} \epsilon_n d^\dagger_{ns} d_{ns} - E_S \boldsymbol{S}^2 - E_Z S^z + E_C \left(N - \mathcal{N}\right)^2 . \qquad (1)$$

Here, $N = \sum_{s,n} d^\dagger_{ns} d_{ns}$ is the total number of electrons occupying the levels $n = \pm 1$, operator $\boldsymbol{S} = \sum_{nss'} d^\dagger_{ns} \left(\boldsymbol{\sigma}_{ss'}/2\right) d_{ns'}$ is the corresponding total spin ($\boldsymbol{\sigma}$ are the Pauli matrices), and the parameters E_S, $E_Z = g\mu_B B$, and E_C are the exchange, Zeeman, and charging energies respectively [7]. We restrict our attention to the very middle of a Coulomb blockade valley with an even number of electrons in the dot (that is modelled by setting the dimensionless gate voltage $\mathcal{N}$ to $\mathcal{N} = 2$). We assume that the level spacing δ is tunable, *e.g.*, by means of a magnetic field B: $\delta = \delta(B)$, and that $\delta(0) > 2E_S$ (which ensures that the dot is non-magnetic for $B = 0$).

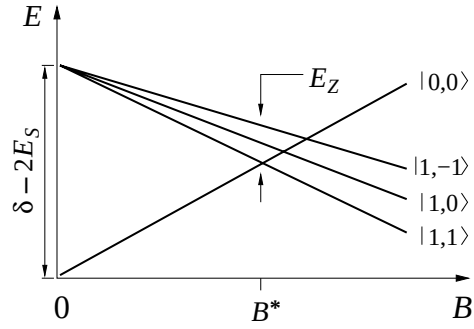

Fig. 1. Typical picture of the singlet-triplet transition in the ground state of a quantum dot.

The lowest–energy singlet state and the three components of the competing triplet state can be labeled as $|S, S^z\rangle$ in terms of the total spin S and its z–projection S_z,

$$\begin{aligned}
|1,1\rangle &= d^\dagger_{+1\uparrow} d^\dagger_{-1\uparrow} |0\rangle, \\
|1,-1\rangle &= d^\dagger_{+1\downarrow} d^\dagger_{-1\downarrow} |0\rangle, \\
|1,0\rangle &= \frac{1}{\sqrt{2}} \left(d^\dagger_{+1\uparrow} d^\dagger_{-1\downarrow} + d^\dagger_{+1\downarrow} d^\dagger_{-1\uparrow} \right) |0\rangle, \\
|0,0\rangle &= d^\dagger_{-1\uparrow} d^\dagger_{-1\downarrow} |0\rangle,
\end{aligned} \qquad (2)$$

where $|0\rangle$ is the state with the two levels empty. According to (1), the energies of these states satisfy

$$E_{|S,S^z\rangle} - E_{|0,0\rangle} = K_0 S - E_Z S^z, \qquad (3)$$

where $K_0 = \delta - 2E_S$. Since $\delta > 2E_S$, the ground state of the dot at $B = 0$ is a singlet $|0,0\rangle$. Finite field shifts the singlet and triplet states due to the orbital

effect, and also leads to Zeeman splitting of the components of the triplet. As B is varied, the level crossings occur (see Fig. 1). The first such crossing takes place at $B = B^*$, satisfying the equation

$$\delta(B^*) - E_Z(B^*) = 2E_S. \tag{4}$$

At this point, the two states, $|0,0\rangle$ and $|1,1\rangle$, form a doubly degenerate ground state, see Fig. 1.

If leads are attached to the dot, the dot-lead tunneling results in the hybridization of the degenerate (singlet and triplet) states. The characteristic energy scale T_0 associated with the hybridization can be in different relations with the Zeeman splitting at field $B = B^*$.

If $E_Z(B^*) \ll T_0$, then the Zeeman splitting between the triplet states can be neglected, and at the $B = B^*$ point all *four* states (2) can be considered as degenerate. Theory for this case is presented below in Section 2.3. This limit adequately describes a quantum dot formed in a two-dimensional electron gas (2DEG) at the GaAs-AlGaAs interface, subject to a magnetic field, see Section 3.1. Energy E_Z can be neglected due to the smallness of the electron g-factor in GaAs.

Alternatively, the orbital effect of the magnetic field (B-dependence of δ) may be very weak due to the reduced dimensionality of the system, while the g-factor is not suppressed, yielding an appreciable Zeeman effect even in a magnetic field of a moderate strength. This limit of the theory, see Section 2.4, corresponds to single-wall carbon nanotubes, which have very small widths of about 1.4 nm and $g = 2.0$. Measurements with carbon nanotubes are presented in Section 3.2.

In order to study the transport problem, we need to introduce into the model the Hamiltonian of the leads and a term that describes the tunneling. We choose them in the following form:

$$H_l = \sum_{\alpha nks} \xi_k c^\dagger_{\alpha nks} c_{\alpha nks}, \tag{5}$$

$$H_T = \sum_{\alpha nn' ks} t_{\alpha nn'} c^\dagger_{\alpha nks} d_{n's} + \text{H.c.} \tag{6}$$

Here $\alpha = R, L$ for the right/left lead, and $n = \pm 1$ for the two orbitals participating in the singlet-triplet transition; k labels states of the continuum spectrum in the leads, and s is the spin index. In writing (5)-(6), we had in mind the vertical dot device, where the potential creating lateral confinement of electrons most probably does not vary much over the thickness of the dot[8]. Therefore we have assumed that the electron orbital motion perpendicular to the axis of the device can be characterised by the same quantum number n inside the dot and in the leads. Presence of two orbital channels $n = \pm 1$ is important for the description of the Kondo effect at the singlet-triplet transition, that is, when the orbital effect of the magnetic field dominates. In the opposite case of large Zeeman splitting, the problem is reduced straightforwadly to the single-channel one, as we will see in Section 2.4 below.

2.1 Effective Hamiltonian

We will demonstrate the derivation of the effective low-energy Hamiltonian under the simplifying assumption [9],[10]

$$t_{\alpha nn'} = t_\alpha \delta_{nn'}. \tag{7}$$

This assumption, on one hand, greatly simplifies the calculations, and, on the other hand, is still general enough to capture the most important physical properties [11].

It is convenient to begin the derivation by performing a rotation[12] in the R-L space

$$\begin{pmatrix} \psi_{nks} \\ \phi_{nks} \end{pmatrix} = \frac{1}{\sqrt{t_L^2 + t_R^2}} \begin{pmatrix} t_R & t_L \\ -t_L & t_R \end{pmatrix} \begin{pmatrix} c_{Rnks} \\ c_{Lnks} \end{pmatrix}, \tag{8}$$

after which the ϕ field decouples:

$$H_T = \sqrt{t_L^2 + t_R^2} \sum_{nks} \psi^\dagger_{nks} d_{ns} + \text{H.c.} \tag{9}$$

The differential conductance at zero bias G can be related, using Eq. (8), to the amplitudes of scattering $A_{ns\to n's'}$ of the ψ–particles

$$G = \lim_{V\to 0} dI/dV = \frac{e^2}{h} \left(\frac{2t_L t_R}{t_L^2 + t_R^2} \right)^2 \sum_{nn'ss'} |A_{ns\to n's'}|^2. \tag{10}$$

The next step is to integrate out the virtual transitions to the states with $\mathcal{N} \pm 1$ electrons by means of the Schrieffer-Wolff transformation or, equivalently, by the Brillouin–Wigner perturbation theory. This procedure results in the effective low-energy Hamiltonian in which the transitions between the states (2) are described by of the operators

$$\boldsymbol{S}_{nn'} = \mathcal{P} \sum_{ss'} d^\dagger_{ns} \frac{\boldsymbol{\sigma}_{ss'}}{2} d_{n's'} \mathcal{P},$$

where $\mathcal{P} = \sum_{S,S^z} |S, S^z\rangle\langle S, S^z|$ is the projection operator onto the system of states (2). The operators $\boldsymbol{S}_{nn'}$ may be conveniently written in terms of two fictitious 1/2-spins $\boldsymbol{S}_{1,2}$. The idea of mapping comes from the one-to-one correspondence between the set of states (2) and the states of a two-spin system:

$$\begin{aligned} &|1,1\rangle \Longleftrightarrow |\uparrow_1\uparrow_2\rangle, \quad |1,-1\rangle \Longleftrightarrow |\downarrow_1\downarrow_2\rangle, \\ &|1,0\rangle \Longleftrightarrow \frac{1}{\sqrt{2}} \left(|\uparrow_1\downarrow_2\rangle + |\downarrow_1\uparrow_2\rangle \right), \\ &|0,0\rangle \Longleftrightarrow \frac{1}{\sqrt{2}} \left(|\uparrow_1\downarrow_2\rangle - |\downarrow_1\uparrow_2\rangle \right). \end{aligned}$$

We found the following relations:

$$\begin{aligned} \boldsymbol{S}_{nn} &= \frac{1}{2}\left(\boldsymbol{S}_1 + \boldsymbol{S}_2\right) = \frac{1}{2}\boldsymbol{S}_+, \\ \sum_n \boldsymbol{S}_{-n,n} &= \frac{1}{\sqrt{2}}\left(\boldsymbol{S}_1 - \boldsymbol{S}_2\right) = \frac{1}{\sqrt{2}}\boldsymbol{S}_-, \\ \sum_n in\mathbf{S}_{-n,n} &= \sqrt{2}\left[\boldsymbol{S}_1 \times \boldsymbol{S}_2\right] = \sqrt{2}\mathbf{T}. \end{aligned} \tag{11}$$

In terms of $\mathrm{S}_{1,2}$, the effective Hamiltonian takes the form:

$$H = \sum_{nks} \xi_k \psi^\dagger_{nks}\psi_{nks} + K\left(\boldsymbol{S}_1 \cdot \boldsymbol{S}_2\right) - E_Z S^z_+ + \sum_n H_n, \tag{12}$$

$$\begin{aligned} H_n = {} & J\left(\boldsymbol{s}_{nn} \cdot \boldsymbol{S}_+\right) + Vn\rho_{nn}\left(\boldsymbol{S}_1 \cdot \boldsymbol{S}_2\right) \\ & + \frac{I}{\sqrt{2}}\left[\left(\boldsymbol{s}_{-n,n} \cdot \boldsymbol{S}_-\right) + 2in\left(\boldsymbol{s}_{-n,n} \cdot \mathbf{T}\right)\right]. \end{aligned} \tag{13}$$

Here we introduced the particle and spin densities in the continuum:

$$\rho_{nn} = \sum_{kk's} \psi^\dagger_{nks}\psi_{nk's}, \;\; \boldsymbol{s}_{nn'} = \sum_{kk'ss'} \psi^\dagger_{nks}\frac{\boldsymbol{\sigma}_{ss'}}{2}\psi_{n'k's'}.$$

The bare values of the coupling constants are

$$J = I = 2V = 2\left(t_L^2 + t_R^2\right)/E_C. \tag{14}$$

Note that the Schrieffer-Wolff transformation also produces a small correction to the energy gap Δ between the states $|1,1\rangle$ and $|0,0\rangle$,

$$\Delta = E_{|1,1\rangle} - E_{|0,0\rangle} = K - E_Z, \tag{15}$$

so that K differs from its bare value K_0, see (3). However, this difference is not important, since it only affects the value of the control parameter at which the singlet-triplet transition occurs, but not the nature of the transition.

We did not include into (1)-(13) the free-electron Hamiltonian of the ϕ-particles [see Eq. (8)], as well as some other terms, that are irrelevant for the low energy renormalization. The contribution of these terms to the conductance is featureless at the energy scale of the order of T_0 (see the next section), where the Kondo resonance develops.

At this point, it is necessary to discuss some approximations tacitly made in the derivation of (1)-(13). First of all, we entirely ignored the presence of many energy levels in the dot, and took into account the low-energy multiplet (2) only. The multi-level structure of the dot is important at the energies above δ, while the Kondo effect physics emerges at the energy scale well below the single-particle level spacing [13]. The high-energy states result merely in a renormalization of the parameters of the effective low-energy Hamiltonian. One only needs to consider this renormalization for deriving the relation between the parameters t_L

and t_R of the low-energy Hamiltonian (1), (5) and (6) and the "bare" constants of the model defined in a wide bandwidth ϵ_F. On the other hand, using the effective low-energy Hamiltonian, one can calculate, in principle, the observable quantities such as conductance $G(T)$ and other susceptibilities of the system at low temperatures ($T \ll \delta$), and establish the relations between them, which is our main goal.

Note that the Hamiltonian (1)-(13) resembles that of the two-impurity Kondo model, for which $H_n = J_n (\boldsymbol{s}_{nn} \cdot \boldsymbol{S}_+) + I (\boldsymbol{s}_{-n,n} \cdot \boldsymbol{S}_-)$ and the parameter K characterizes the strength of the RKKY interaction [14]. It is known that the two-impurity Kondo model may undergo a phase transition at some special value of K [14]. At this point, the system may exhibit non-Fermi liquid properties. However, one can show [10], using general arguments put forward in [14], that the model (1)-(13) does not have the symmetry that warrants the existence of the non Fermi liquid state. This allows one to apply the local Fermi liquid description [15] to study the properties of the system at $T = 0$. In the next section, we will concentrate on the experimentally relevant perturbative regime.

2.2 Scaling Analysis

To calculate the differential conductance in the leading logarithmic approximation, we apply the "poor man's" scaling technique [16]. The procedure consists of a perturbative elimination of the high-energy degrees of freedom and yields the and yields the set of scaling equations

$$\begin{aligned} dJ/d\mathcal{L} &= \nu \left(J^2 + I^2\right), \\ dI/d\mathcal{L} &= 2\nu I \left(J + V\right), \\ dV/d\mathcal{L} &= 2\nu I^2 \end{aligned} \tag{16}$$

for the renormalization of the coupling constants with the decrease of the high energy cutoff D. Here $\mathcal{L} = \ln(\delta/D)$, and ν is the density of states in the leads; the initial value of D is $D = \delta$, see the discussion after Eq. (15). The initial conditions for (16), $J(0)$, $I(0)$, and $V(0)$ are given by Eq. (14). The scaling procedure also generates non-logarithmic corrections to K. In the following we absorb these corrections in the re-defined value of K. Equations (16) are valid in the perturbative regime and as long as

$$D \gg |K|, E_Z, T.$$

At certain value of $\mathcal{L}$, $\mathcal{L} = \mathcal{L}_0 = \ln(\delta/T_0)$, the inverse coupling constants simultaneously reach zero:

$$1/J(\mathcal{L}_0) = 1/I(\mathcal{L}_0) = 1/V(\mathcal{L}_0) = 0.$$

This defines the characteristic energy scale of the problem:

$$T_0 = \delta \exp\left[-\tau_0/\nu J\right]. \tag{17}$$

Here τ_0 is a parameter that depends on the initial conditions and should be found numerically. We obtained $\tau_0 = 0.36$ (see Fig. 2).

It is instructive to compare T_0 with the Kondo temperature $T_K^{\rm odd}$ in the adjacent Coulomb blockade valleys with $N = odd$. In this case, only electrons from one of the two orbitals $n = \pm 1$ are involved in the effective Hamiltonian, which takes the form of the 1-channel $S = 1/2$ Kondo model with the exchange amplitude $J_{\rm odd} = 4(t_L^2 + t_R^2)/E_C = 2J$, see Eq. (14). Therefore, $T_K^{\rm odd}$ is given by the same expression (3.2) as T_0, but with $\tau_0 = 1/2$. For realistic values of the parameters $T_0 = 300\ mK$, $\delta = 3\ meV$ we obtain $T_K^{\rm odd} \approx 120\ mK$. This estimate is in a reasonable agreement with the experimental data, see Section 3.1 below.

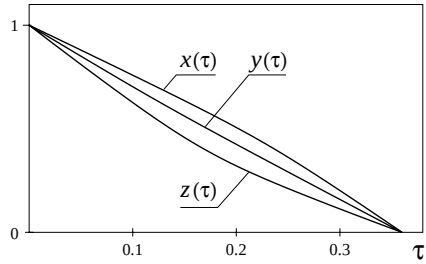

Fig. 2. Numerical solution of the scaling equations. The RG equations (16) are rewritten in terms of the new variable $\tau = \nu J(0) \ln(\delta/D)$ and the new functions $x(\tau) = J(0)/J(\tau)$, $y(\tau) = I(0)/I(\tau)$, $z(\tau) = V(0)/V(\tau)$ as $dx/d\tau = -(1 + x^2/y^2)$, $dy/d\tau = -(2y/x + y/z)$, $dz/d\tau = -4z^2/y^2$. The three functions reach zero simultaneously at $\tau = \tau_0 = 0.36$.

The solution of the RG equations (16) can now be expanded near $\mathcal{L} = \mathcal{L}_0$. To the first order in $\mathcal{L}_0 - \mathcal{L} = \ln D/T_0$, we obtain

$$\frac{1}{\nu J(\mathcal{L})} = \frac{\sqrt{\lambda}}{\nu I(\mathcal{L})} = \frac{\lambda - 1}{2\nu V(\mathcal{L})} = (\lambda + 1) \ln(D/T_0), \tag{18}$$

where

$$\lambda = 2 + \sqrt{5} \approx 4.2.$$

It should be emphasized that, unlike τ_0, the constant λ is universal in the sense that its value is not affected if the restriction (7) is lifted [11].

Eq. (18) can be used to calculate the differential conductance at high temperature $T \gg |K|, E_Z, T_0$. In this regime, the coupling constants are still small, and the conductance is obtained by applying a perturbation theory to the Hamiltonian (1)-(13) with renormalized parameters (18), taken at $D = T$, and using (10). This yields

$$G/G_0 = \frac{A}{\left[\ln(T/T_0)\right]^2}, \tag{19}$$

where

$$A = \left(3\pi^2/8\right)(\lambda + 1)^{-2} \left[1 + \lambda + (\lambda - 1)^2/8\right] \approx 0.9$$

is a numerical constant, and

$$G_0 = \frac{4e^2}{h}\left(\frac{2t_L t_R}{t_L^2 + t_R^2}\right)^2 . \tag{20}$$

As temperature is lowered, the scaling trajectory (16) terminates either at $D \sim \max\{|K|, E_Z\} \gg T_0$, or when the system approaches the strong coupling regime $D \sim T_0 \gg |K|, E_Z$. It turns out that the two limits of the theory, $E_Z \ll T_0$ and $E_Z \gg T_0$, describe two distinct physical situations, which we will discuss separately.

2.3 Singlet–Triplet Transition

In this section, we assume that the Zeeman energy is negligibly small compared to all other energy scales. At high temperature $T \gg |K|, T_0$, the conductance is given by Eq. (19). At low temperature $T \lesssim |K|$ and away from the singlet-triplet degeneracy point, $|K| \gg T_0$, the RG flow yielding Eq. (19) terminates at energy $D \sim |K|$. On the *triplet* side of the transition ($K \ll -T_0$), the two spins $\boldsymbol{S}_{1,2}$ are locked into a triplet state. The system is described by the effective 2-channel Kondo model with $S = 1$ impurity, obtained from Eqs. (1)-(13) by projecting out the singlet state and dropping the no longer relevant potential scattering term:

$$H_{\text{triplet}} = \sum_{nks} \xi_k \psi^\dagger_{nks}\psi_{nks} + J\sum_n (\boldsymbol{s}_{nn}\cdot\boldsymbol{S})\,; \tag{21}$$

here J is given by the solution $J(\mathcal{L})$ of Eq. (16), taken at $\mathcal{L} = \mathcal{L}^* = \ln(\delta/|K|)$, which corresponds to $D = |K|$.

As D is lowered below $|K|$, the renormalization of the exchange amplitude J is governed by the standard RG equation [16]

$$dJ/d\mathcal{L} = \nu J^2, \tag{22}$$

where $\mathcal{L} = \ln(\delta/D) > \mathcal{L}^*$. Eq. (22) is easily integrated with the result

$$1/\nu J(\mathcal{L}) - 1/\nu J(\mathcal{L}^*) = \mathcal{L} - \mathcal{L}^*.$$

This can be also expressed in terms of the running bandwidth D and the Kondo temperature

$$T_k = |K| \exp\left[-1/\nu J(\mathcal{L}^*)\right]$$

as $1/\nu J(\mathcal{L}) = \ln(D/T_k)$.

Obviously, T_k depends on $|K|$. Using asymptotes of $J(\mathcal{L})$, see Eq. (18), we obtain the scaling relation

$$T_k/T_0 = (T_0/|K|)^\lambda\,. \tag{23}$$

Eq. (23) is valid not too far from the transition point, where the inequality

$$1 \lesssim |K|/T_0 \ll (\delta/T_0)^\mu,\ \mu \approx 0.24 \tag{24}$$

is satisfied. Here, μ is a numerical constant, which depends on τ_0, and therefore is not universal [see the remark after Eq. (18)]. For larger values of $|K|$ (but still smaller than δ), $T_k \propto 1/|K|$ [11]. Finally, for $|K| = \delta$, T_k is given by Eq. (3.2) with $\tau_0 = 1$. According to (23), T_k decreases very rapidly with $|K|$. For example, for $T_0 = 300\ mK$ and $\delta = 3\ meV$ Eq. (23) describes fall of T_k by an order of magnitude within the limits of its validity (24). For $|K| = \delta$ one obtains $T_k \approx 5\ mK$, which is well beyond the reach of the present day experiments.

For a given $|K|$, $T_0 \lesssim |K| \lesssim \delta$, the differential conductance can be cast into the scaling form,

$$G/G_0 = F\left(T/T_k\right) \tag{25}$$

where $F(x)$ is a smooth function that interpolates between $F(0) = 1$ and $F(x \gg 1) = \left(\pi^2/2\right)(\ln x)^{-2}$. It coincides with the scaled resistivity

$$F(T/T_K) = \rho(T/T_K)/\rho(0)$$

for the symmetric two–channel $S = 1$ Kondo model. The conductance at $T = 0$ (the unitary limit value), G_0, is given above in Eq. (13).

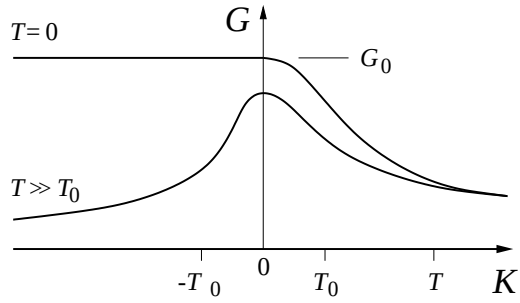

Fig. 3. Linear conductance near a singlet-triplet transition. At high temperature G exhibits a peak near the transition point. At low temperature G reaches the unitary limit at the triplet side of the transition, and decreases monotonously at the singlet side. The two asymptotes merge at $K \gg T, T_0$.

On the *singlet* side of the transition, $K \gg T_0$, the scaling terminates at $D \sim K$, and the low-energy effective Hamiltonian is

$$H_{\text{singlet}} = \sum_{nks} \xi_k \psi^\dagger_{nks} \psi_{nks} - \frac{3}{4} V \sum_n n \rho_{nn},$$

where V is $V(\mathcal{L})$ [see Eq. (16)] taken at $\mathcal{L} = \mathcal{L}^*$. The temperature dependence of the conductance saturates at $T \ll K$, reaching the value

$$G/G_0 = \frac{B}{\left[\ln(K/T_0)\right]^2}, \quad B = \left(\frac{3\pi}{8}\frac{\lambda - 1}{\lambda + 1}\right)^2 \approx 0.5. \tag{26}$$

Note that at $T = 0$ Eqs. (25) and (26) predict different dependence on the parameter K which is used for tuning thorugh the transition. At positive K,

conductance decreases with the increase of K; at $K \ll -T_0$ conductance $G = G_0$ and does not depend of K. Although there is no reason for the function $G(K)$ to be discontinious [10], it is obviously a *non-analytical* function of K, see Fig. 3.

The above results are for the linear conductance G. At $T = 0$, G is a monotonous function of K, at high temperature $T \gg T_0$ the conductance develops a peak at the singlet-triplet transition point $K = 0$. We now discuss shortly out-of-equilibrium properties. When the system is tuned to the transition point $K = 0$, the differential conductance dI/dV exhibits a peak at zero bias, whose width is of the order of T_0. For finite K the peak splits in two, located at *finite* bias $eV = \pm K$. The mechanism of this effect is completely analogous to the Zeeman splitting of the usual Kondo resonance [4],[2]: $|K|$ is the energy cost of the processes involving a singlet-triplet transition. This cost can be covered by applying a finite voltage $eV = \pm K$, so that the tunneling electron has just the right amount of extra energy to activate the singlet-triplet transition prosesses described by the last two terms in (13). The split peaks gradually disappear at large $|K|$ due to the nonequilibrium-induced decoherence [17],[18].

2.4 Transition Driven by Zeeman Splitting

If the Zeeman energy is large, the RG flow (16) terminates at $D \sim E_Z$. The effective Hamiltonian, valid at the energies $D \lesssim E_Z$ is obtained by projecting (1)-(13) onto the states $|1,1\rangle$ and $|0,0\rangle$. These states differ by a flip of a spin of a single electron (see Fig. 4), and are the counterparts of the spin-up and spin-down states of $S = 1/2$ impurity in the conventional Kondo problem. It is therefore convenient to switch to the notations

$$|1,1\rangle = |\uparrow\rangle, \quad |0,0\rangle = |\downarrow\rangle, \tag{27}$$

and to describe the transitions between the two states in terms of the spin-like operator

$$\widetilde{\boldsymbol{S}} = \frac{1}{2}\sum_{ss'} |s\rangle \boldsymbol{\sigma}_{ss'} \langle s'|,$$

built from the states (27).

Projecting onto the sates (27), we obtain from (1)-(13)

$$\begin{aligned} H = & \sum_{nks} \xi_k \psi^\dagger_{nks}\psi_{nks} + \Delta \widetilde{S}^z \\ & + \sum_n \left[J s^z_{nn} \left(\widetilde{S}^z + 1/2\right) + V n \rho_{nn} \left(\widetilde{S}^z - 1/4\right)\right] \\ & - I\left(s^+_{1,-1}\widetilde{S}^- + \text{H.c.}\right), \end{aligned} \tag{28}$$

where Δ was introduced above in Eq. (15). It is now convenient to transform (28) to a form which is diagonal in the orbital indexes n. This is achieved simply by relabeling the fields according to

$$\begin{aligned} \psi_{+1,k,\uparrow} = a_{k,\uparrow},\ \psi_{-1,k,\downarrow} = -a_{k,\downarrow}, \\ \psi_{-1,k,\uparrow} = b_{k,\uparrow},\ \psi_{+1,k,\downarrow} = -b_{k,\downarrow}, \end{aligned} \tag{29}$$

which yields

$$\begin{aligned} H = \; & H_0 + \Delta \widetilde{S}^z \\ & + V_a s_a^z + J_z s_a^z \widetilde{S}^z + \frac{1}{2} J_\perp \left(s_a^+ \widetilde{S}^- + s_a^- \widetilde{S}^+ \right) \\ & + V_b s_b^z + J_z' s_b^z \widetilde{S}^z, \end{aligned} \tag{30}$$

where H_0 is a free-particle Hamiltonian for a, b electrons, and $\boldsymbol{s}_a$ is the spin density for a electrons, $\boldsymbol{s}_a = \sum_{kk'ss'} a_{ks}^\dagger \left(\boldsymbol{\sigma}_{ss'}/2\right) a_{k's'}$ (with a similar definition for $\boldsymbol{s}_b$). The coupling constants in (30),

$$\begin{aligned} & V_a = (J - V)/2, \; J_z = J + 2V, \; J_\perp = 2I, \\ & V_b = (J + V)/2, \; J_z' = J - 2V \end{aligned} \tag{31}$$

are expressed through the solutions of the RG equations (16) taken at $\mathcal{L} = \mathcal{L}^{**} = \ln(\delta/E_Z)$.

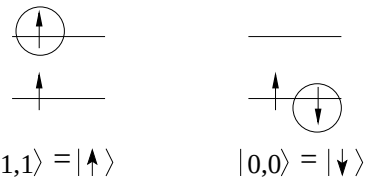

Fig. 4. The ground state doublet in case of a large Zeeman splitting. The states $|1,1\rangle$ and $|0,0\rangle$ differ by flipping a spin of a single electron (marked by circles).

The operators in b-dependent part of (30) are not relevant for the low energy renormalization. At low enough temperature (satisfying the condition $\ln(T/T_Z) \ll (\nu J_z')^{-1}$, $(\nu V_b)^{-1}$, where T_Z is the Kondo temperature), their contribution to the conductance becomes negligible compared to the contribution from the a-dependent terms. This allows us to drop the b-dependent part of (30). Suppressing the (now redundant) subscript of the operators s_a^i, we are left with the Hamiltonian of a one-channel $S = 1/2$ anisotropic Kondo model,

$$H = H_0 + \Delta \widetilde{S}^z + V_a s^z + J_z s^z \widetilde{S}^z + \frac{J_\perp}{2} (s^+ \widetilde{S}^- + \text{H.c.}). \tag{32}$$

Eq. (32) emerged as a limiting case of a more general two-channel model (1)-(13). It should be noticed, however, that the same effective Hamiltonian (32) appears when one starts with the single-channel model from the very beginning [19].

A finite magnetic field singles out the z-direction, so that the spin–rotational symmetry is absent in (1)-(13). This property is preserved in (32). Indeed, even for $J_z = J_\perp$, Eq. (32) contains term $V_\psi s^z$ which has the meaning of a magnetic field acting *locally* on the conduction electrons at the impuirity site. The main effect of this term is to produce a correction to Δ, through creating a non-zero expectation value $\langle s^z \rangle$ [20]. This results in a correction to Δ. Fortunately,

this correction is not important, since it merely shifts the degeneracy point. In addition, this term leads to insignificant corrections to the density of states [19].

Let us now examine the relation between J_z and $J_\perp$. It follows from Eqs. (14) and (31), that at $E_Z = \delta$ the exchange is isotropic: $J_z = J_\perp$. Moreover, it turns out that if E_Z is so close to δ, that Eqs. (16) can be linearized near the weak coupling fixed point $\mathcal{L} = 0$, the corrections to $J_z, J_\perp$ are such that the isotropy of exchange is preserved:

$$J_z = J_\perp = 2J(0)\left[1 + \frac{3}{4}\nu J(0)\ln(\delta/E_Z)\right], \tag{33}$$

where $J(0)$ is given by (14). This expression is valid as long as the logarithmic term in the r.h.s. is small: $\nu J(0)\ln(\delta/E_Z) \ll 1$. Using (33) and (3.2), one obtains the Kondo temperature T_Z, which for $J_z = J_\perp$ is given by

$$T_Z = E_Z \exp[-1/\nu J_z] = E_Z(\delta/E_Z)^{3/8}(T_0/\delta)^{1/2\tau_0}$$

Note that for $E_Z = \delta$, T_Z coincides with the Kondo temperature $T_K^{\rm odd}$ in the adjacent Coulomb blockade valleys with odd number of electrons [19], see the discussion after Eq. (3.2) above.

Note that the anisotropy of the exchange merely affects the value of T_Z (which can be written explicitely for arbitrary J_z and $J_\perp$ [21]). In the universal regime (when T approaches T_Z), the exchange can be considered isotropic. This is evident from the scaling equations [16]

$$dJ_z/d\mathcal{L} = \nu J_\perp^2,\ dJ_\perp/d\mathcal{L} = \nu J_z J_\perp,\ \mathcal{L} > \mathcal{L}^{**} \tag{34}$$

where $\mathcal{L} > \mathcal{L}^{**} = \ln(\delta/E_Z)$, whose solution approaches the line $J_z = J_\perp$ at large $\mathcal{L}$.

According to the discussion above, the term $V_\psi s^z$ in Eq. (32) can be neglected. As a results, (32) acquires the form of the anisotropic Kondo model, with Δ playing the part of the Zeeman splitting of the impurity levels. This allows us to write down the expression for the linear conductance at once. Regardless the initial anisotropy of the exchange constants in Eq. (32), the conductance for $\Delta = 0$ in the universal regime (when T approaches T_Z or lower) is given by

$$G = G_{0Z} f\left(T/T_Z\right), \tag{35}$$

where $f(x)$ is a smooth function interpolating between $f(0) = 1$ and $f(x \gg 1) = (3\pi^2/16)(\ln x)^{-2}$. Function $f\left(T/T_Z\right)$ coincides with the scaled resistivity for the one-channel $S = 1/2$ Kondo model and its detailed shape is known from the numerical RG calculations [22]. The conductance at $T = 0$,

$$G_{0Z} = \frac{2e^2}{h}\left(\frac{2t_L t_R}{t_L^2 + t_R^2}\right)^2, \tag{36}$$

is by a factor of 2 smaller than G_0 [see Eq. (13)]; G_0 includes contributions from two channels and therefore is twice as large as the single-channel result (36). At

finite $\Delta \gg T_Z$, the scaling trajectory (34) terminates at $D \sim \Delta$. As a result, at $T \lesssim \Delta$ the conductance is temperature-independent, and for $J_z = J_\perp$

$$G = G_{0Z} f(\Delta/T_Z) = G_{0Z} \frac{3\pi^2/16}{[\ln(\Delta/T_Z)]^2}.$$

The effect of the de-tuning of the magnetic field from the degeneracy point $\Delta \neq 0$ on the differential conductance away from equilibrium is similar to the effect the magnetic field has on the usual Kondo resonance [4],[2]. For example, consider the case, relevant for the experiments on the carbon nanotubes, see section 3.2, when the exchange energy E_S [see Eq. (1)] is negligibly small. When sweeping magnetic field from $B = -\infty$ to $B = +\infty$, the degeneracy between the singlet state of the dot and a component of the triplet is reached twice, at $B = B^*$ and $B = -B^*$, when $|E_Z| \approx \delta$. If the field is tuned to $B = \pm B^*$, then the differential conductance dI/dV has a peak at zero bias. At a finite difference $|B| - |B^*|$ this peak splits in two located at $eV = \pm g\mu_B(|B| - |B^*|)$.

3 Experiments

3.1 GaAs Quantum Dots

Here, we discuss the case of a quantum dot with $N = even$ in a situation where the last two electrons occupy either a spin singlet or a spin triplet state. The transition between singlet and triplet state is controlled with an external magnetic field. The range of the magnetic field is small ($B \sim 0.2\ T$, $g\mu_B B \sim 5\ \mu V$) such that the Zeeman energy can be neglected and that the triplet state is fully degenerate[23]. The theory for this situation was described in section 2.3.

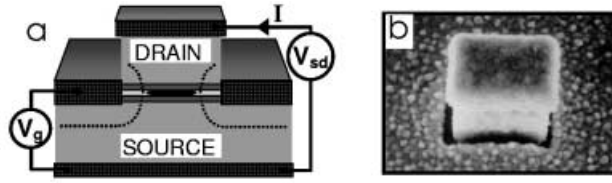

Fig. 5. (**a**) Cross-section of rectangular quantum dot. The semiconductor material consists of an undoped AlGaAs(7nm)/InGaAs(12nm)/AlGaAs(7nm) double barrier structure sandwiched between n-doped GaAs source and drain electrodes. A gate electrode surrounds the pillar and is used to control the electrostatic confinement in the quantum dot. A dc bias voltage, V, is applied between source and drain and current, I, flows vertically through the pillar. The gate voltage, V_g, can change the number of confined electrons, N, one-by-one. A magnetic field, B, is applied along the vertical axis. (**b**) Scanning electron micrograph of a quantum dot with dimensions $0.45 \times 0.6\ \mu m^2$ and height of $\sim 0.5\ \mu m$.

The quantum dot has the external shape of a rectangular pillar (see Fig. 5) and an internal confinement potential close to a two-dimensional ellipse [8]. The

tunnel barriers between the quantum dot and the source and drain electrodes are thinner than in other devices such that higher-order tunneling processes are enhanced. Fig. 6 shows the linear response conductance G versus gate voltage V_g, and magnetic field B. Dark regions have low conductance and correspond to the regimes of Coulomb blockade for $N = 3$ to 10. Light stripes represent Coulomb peaks as high as $\sim e^2/h$. The B-dependence of the first two lower stripes reflects the ground-state evolution for $N = 3$ and 4. Their similar B-evolution indicates that the 3rd and 4th electron occupy the same orbital state with opposite spin, which is observed also for $N = 1$ and 2 (not shown). This is not the case for $N = 5$ and 6. The $N = 5$ state has $S = 1/2$, and the corresponding stripe shows a smooth evolution with B. Instead, the stripe for $N = 6$ has a kink at $B = B^* \approx 0.22\ T$. From earlier analyses [8] and from measurements of the excitation spectrum at finite bias V this kink is identified with a transition in the ground state from a spin-triplet to a spin-singlet.

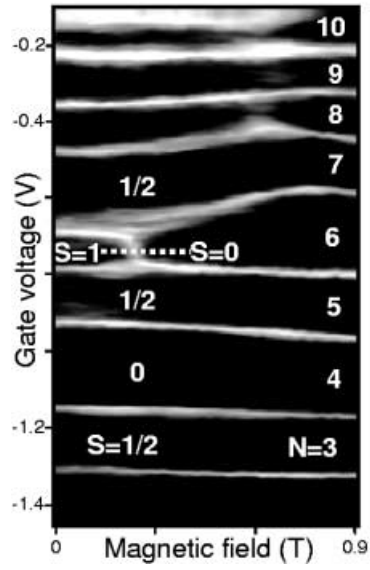

Fig. 6. Gray-scale representation of the linear conductance G versus the gate voltage V_g and the magnetic field B. White stripes denote conductance peaks of height $\sim e^2/h$. Dark regions of low conductance indicate Coulomb blockade. The $N = 6$ ground state undergoes a triplet-to-singlet transition at $B = B^* \approx 0.22\ T$, which results in a conductance anomaly inside the corresponding Coulomb gap.

Strikingly, at the triplet-singlet transition (see Fig. 6) we observe a strong enhancement of the conductance. In fact, over a narrow range around 0.22 T, the Coulomb gap for $N = 6$ has disappeared completely. Note that the change in greyscale along the dashed line in Fig. 6 represents the variation of the conductance with the tuning parameter K, see Fig. 3.

To explore this conductance anomaly, Fig. 7(a) shows the differential conductance, dI/dV versus V, taken at B and V_g corresponding to the intersection of the dotted line and the bright stripe ($B = B^*$) in Fig. 6. The height of the zero-bias resonance decreases logarithmically with T [see Fig. 7(b)]. These are typical fingerprints of the Kondo effect. From FWHM$\approx 30\ \mu V \approx k_B T_0$, we estimate $T_0 \approx 350\ mK$. Note that $k_B T_0/g\mu_B B^* \approx 6$ so that the triplet state is indeed three-fold degenerate on the energy scale of T_0; this justifies an assumption made in Section 2.3 above. Also note that some of the traces in Fig. 7(a) show small short-period modulations which disappear above $\sim 200\ mK$. These are due to a weak charging effect in the GaAs pillar above the dot [24].

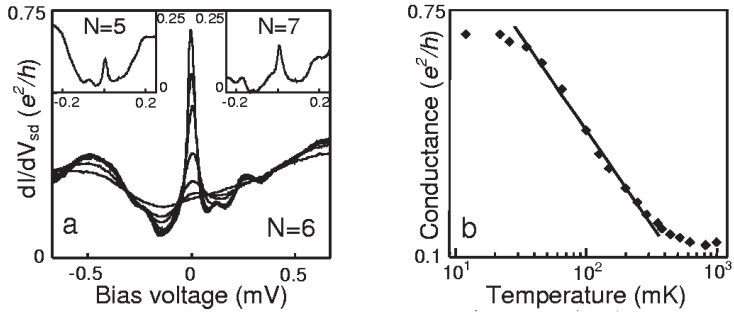

Fig. 7. (**a**) Kondo resonance at the singlet-triplet transition. The dI/dV vs V curves are taken at $V_g = -0.72\ V$, $B = 0.21\ T$ and for $T = 14, 65, 100, 200, 350, 520$, and $810\ mK$. Kondo resonances for $N = 5$ (left inset) and $N = 7$ (right inset) are much weaker than for $N = 6$. (**b**) Peak height of zero-bias Kondo resonance vs T as obtained from (a). The line demonstrates a logarithmic T-dependence, which is characteristic for the Kondo effect. The saturation at low T is likely due to electronic noise.

For $N = 6$ the anomalous T-dependence is found only when the singlet and triplet states are degenerate. Away from the degeneracy, the valley conductance increases with T due to thermally activated transport. For $N = 5$ and 7, zero-bias resonances are clearly observed [see insets to Fig. 7(a)] which are related to the ordinary spin-1/2 Kondo effect. Their height, however, is much smaller than for the singlet-triplet Kondo effect.

We now investigate the effect of lifting the singlet-triplet degeneracy by changing B at a fixed V_g corresponding to the dotted line in Fig. 6. Near the edges of this line, i.e. away from B^*, the Coulomb gap is well developed as denoted by the dark colours. The dI/dV vs V traces still exhibit anomalies, however, now at finite V [see Fig. 8]. For $B = 0.21\ T$ we observe the singlet-triplet Kondo resonance at $V = 0$. At higher B this resonance splits apart showing two peaks at finite V, in agreement with the discussion above (see Section 2.3). For $B \approx 0.39\ T$ the peaks have evolved into steps which may indicate that the spin-coherence associated with the Kondo effect has completely vanished. The upper traces in Fig. 8, for $B < 0.21\ T$, also show peak structures, although less pronounced.

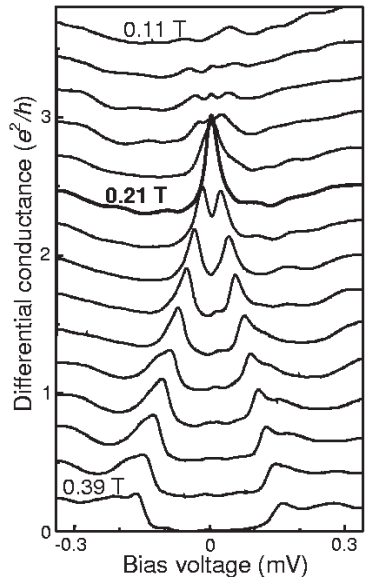

Fig. 8. dI/dV vs V characteristics taken along the dotted line in Fig. 6 at equally spaced magnetic fields $B = 0.11, 0.13, ..., 0.39\ T$. Curves are offset by $0.25\ e^2/h$.

3.2 Carbon Nanotubes

The situation in quantum dots formed in single-wall carbon nanotubes [25], [26],[15],[28] is rather different from that in semiconductor quantum dots. In nanotubes the effect of magnetic field on orbital motion is very weak, because the tube diameter ($\sim 1.4\ nm$) is an order of magnitude smaller than the magnetic length $l_B = (h/eB)^{1/2} \sim 10\ nm$ at a typical maximum laboratory field of $10\ T$. On the other hand, the g-factor is close to its bare value of $g = 2$, compared with $g = 0.44$ in GaAs. Hence the magnetic response of a nanotube dot is determined mainly by Zeeman shifts. As a result, the spins of levels in nanotube dots are easily measured [26],[28], and the ground state is usually (though not always [26]) found to alternate regularly between an $S = 0$ singlet for even electron number N and an $S = 1/2$ doublet for odd N [28],[29]. Moreover, singlet-triplet transitions in nanotubes are likely to be driven by the Zeeman splitting rather than orbital shifts, corresponding to the theory given in section 2.4.

We discuss here the characteristics of a single-walled nanotube device with high contact transparencies, which were presented in more details in [29]. The source and drain contacts are gold, evaporated on top of laser–ablation–grown nanotubes [30] deposited on silicon dioxide. The conducting silicon substrate acts as the gate, as illustrated in Fig. 9. At room temperature the linear conductance G is $1.6\ e^2/h$, almost independent of gate voltage V_g, implying the conductance-dominating nanotube is metallic and defect free, and that the con-

tact transmission coefficients are not much less than unity. At liquid helium temperatures regular Coulomb blockade oscillations develop, implying the formation of a single quantum dot limiting the conductance. However, the conductance in the Coulomb blockade valleys does not go to zero, consistent with high transmission coefficients and a strong coupling of electron states in the tube with the contacts.

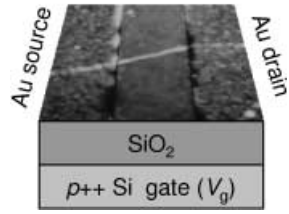

Fig. 9. Schematic of a nanotube quantum dot, incorporating an atomic force microscope image of a typical device (not the same one measured here.) Bridging the contacts, whose separation is 200 nm, is a 2 nm thick bundle of single-walled nanotubes

Fig. 10 shows a grayscale plot of dI/dV versus V and V_g over a small part of the full V_g range at $B = 0$. A regular series of faint "Coulomb diamonds" can be discerned, one of which is outlined by white dotted lines. Each diamond is labeled either E or O according to whether N is even or odd respectively, as determined from the effects of magnetic field. Superimposed on the diamonds are horizontal features which can be attributed to higher-order tunnelling processes that do not change the charge on the dot and therefore are not sensitive to V_g.

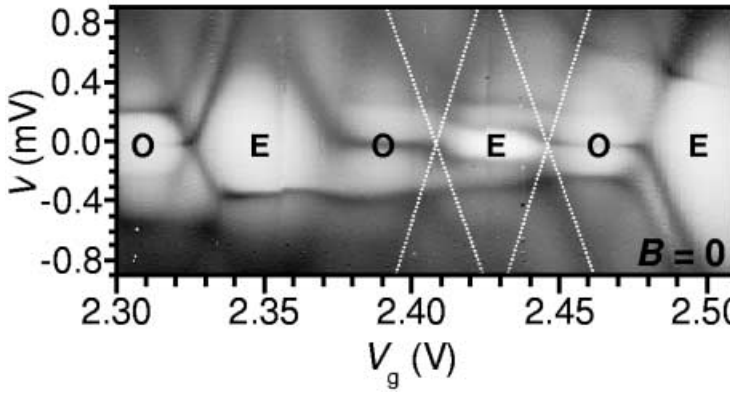

Fig. 10. Grayscale plot of differential conductance dI/dV (darker = more positive) against bias V and gate voltage V_g at a series of magnetic fields and base temperature ($\sim 75\ mK$). Labels 'E' and 'O' indicate whether the number of electrons N in the dot is even or odd (see text).

In Fig. 11(a) we concentrate on an adjacent pair of E and O diamonds in a magnetic field applied perpendicular to the tube. At $B = 0$ the diamond marked with an 'O' has narrow ridge of enhanced dI/dV spanning it at $V = 0$, while that marked with an 'E' does not. An appearence of a ridge at zero bias is consistent with formation of a Kondo resonance which occurs when N is odd (O) but not when it is even (E). This explanation is supported by the logarithmic temperature dependence of the linear conductance in the center of the ridge, as indicated in the inset to Fig. 12(b). At finite B, each zero-bias ridge splits into features at approximately $V = \pm E_Z/e$ as expected for Kondo resonances [4].

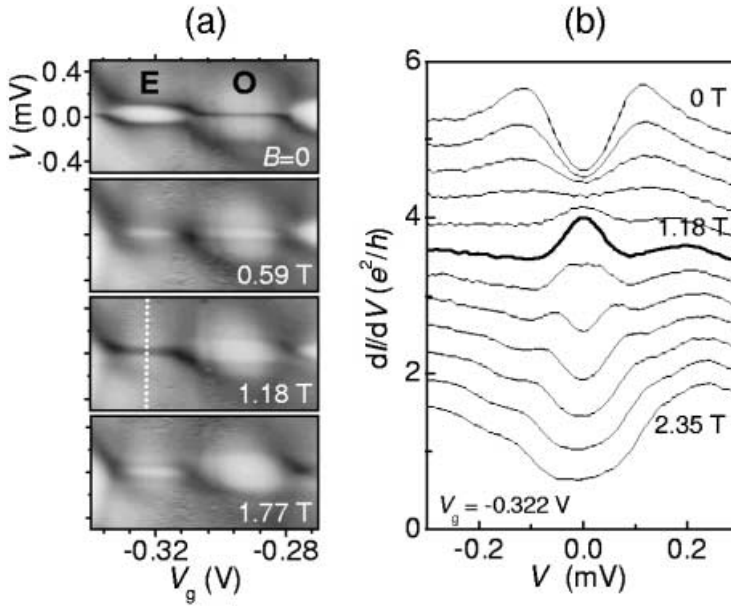

Fig. 11. (**a**) Evolution with magnetic field of adjacent even (E) and odd (O) features of the type seen in Fig. 10. (**b**) dI/dV vs V traces at the center of the E region, at $V_g = -0.322\ V$. The trace at $B = B^* = 1.18\ T$ (bold line) corresponds to the dotted line in (a). The traces are offset from each other by $0.4\ e^2/h$ for clarity.

On the other hand, in the E diamond the horizontal features appear at a finite bias at $B = 0$. The origin of these features can be infered from their evolution with a magnetic field: while the ridge in the O region splits as B increases, the edges of the E 'bubble' move towards $V = 0$, finally merging into a single ridge at $B = B^* = 1.18\ T$. Fig. 11(b) shows the evolution with B of the dI/dV vs V traces from the center of the E region, and the appearance of a zero-bias peak at around $B = 1.18\ T$ (bold trace). This matches what is expected for a Zeeman-driven singlet-triplet transition in the N = even dots (Section 2.4). Further evidence that the peak is a Kondo resonance is provided by its temperature

dependence [Fig. 12(a)], which shows an approximately logarithmic decrease of the peak height (the linear conductance) with T shown in Fig. 12(b).

Based on this interpretation we can deduce that for this particular value of N the energy gap separating the singlet ground state and the lowest-energy triplet state is $\Delta_0 = g\mu_B B^* \approx 137\ \mu eV$. At other even values of N the lowest visible excitations range in energy up to $\sim 400\ \mu eV$. For this device $E_C \sim 500\ \mu eV$. The energy gaps are therefore comparable with the expected single-particle level spacing δ, which is roughly equal to $E_C/3$ in a nanotube dot[15].

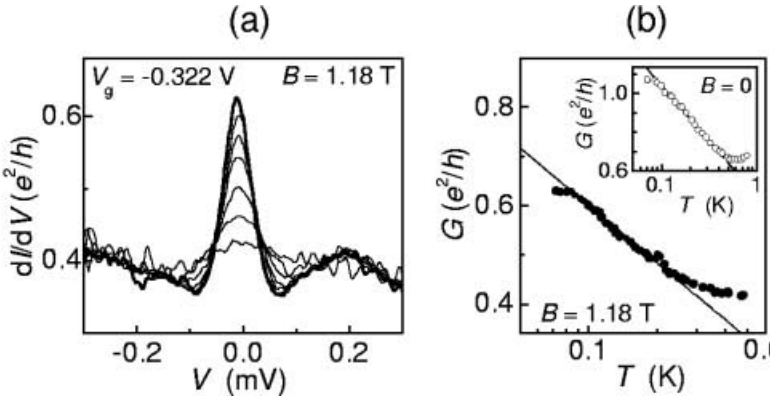

Fig. 12. (**a**) Temperature dependence at $B = B^*$. Here T= base (bold line), 100, 115, 130, 180, 230, and 350 mK. (**b**) Temperature dependence of the linear conductance G (dI/dV at $V = 0$) at $B = B^* = 1.18\ T$. For comparison, $G(T)$ in the center of one of the O-type ridges at $B = 0$ is shown in the inset.

Note that the ridges at finite bias in Fig 11 in E valley are more visible at $B = 0$ than at $B = 0.59\ T$, halfway towards the degeneracy point. A possible explanation is that at $B = 0$ the triplet is not split, and all its components should be taken into account when calculating dI/dV at $B = 0$. This results in an enhancement of dI/dV at $B = 0$, $eV = \delta$, as compared to the value expected from the effective model of Section 2.4, which is valid in the vicinity of $B = B^*$.

Conclusion

Even a moderate magnetic field applied to a quantum dot or a segment of a nanotube can force a transition from the zero-spin ground state ($S = 0$) to a higher-spin state ($S = 1$ in our case). Therefore, the magnetic field may induce the Kondo effect in such a system. This is in contrast with the intuition developed on the conventional Kondo effect, which is destroyed by the applied magnetic field. In this paper we have reviewed the experimental and theoretical aspects of the recently studied magnetic–field–induced Kondo effect in quantum dots. Clearly there is more territory to be explored in the remarkably tuneable systems.

Acknowledgements

We thank our collaborators from Ben Gurion University, Delft University of Technology, Niels Bohr Institute, NTT, and University of Tokyo for their contributions. This work was supported by NSF under Grants DMR-9812340, DMR-9731756, by NEDO joint research program (NTDP-98), and by the EU via a TMR network. LG and MP are grateful to the Max Planck Institute for Physics of Complex Systems (Dresden, Germany), where a part of this paper was written, for the hospitality.

References

1. L. P. Kouwenhoven et al.: In: *Mesoscopic Electron Transport*, ed. by L. L. Sohn et al. (Kluwer, Dordrecht, 1997) pp. 105-214
2. C. B. Duke: *Tunneling in Solids* (New York, 1969); J. M. Rowell: In: *Tunneling Phenomena in Solids*, ed. by E. Burstein and S. Lundqvist (Plenum, New York, 1969)
3. A. F. G. Wyatt: Phys. Rev. Lett. **13**, 401 (1964); R. A. Logan and J. M. Rowell: Phys. Rev. Lett. **13**, 404 (1964)
4. J. Appelbaum: Phys. Rev. Lett. **17**, 91 (1966); Phys. Rev. **154**, 633 (1967); P. W. Anderson: Phys. Rev. Lett. **17**, 95 (1966)
5. J. Kondo: Prog. Theor. Phys. **32**, 37 (1964)
6. D. Goldhaber-Gordon et al.: Nature **391**, 156 (1998); S. M. Cronenwett, T. H. Oosterkamp, and L. P. Kouwenhoven, Science **281**, 540 (1998); J. Schmid et al.: Physica (Amsterdam) **256B-258B**, 182 (1998)
7. I. L. Kurland, I. L. Aleiner, and B. L. Altshuler: preprint cond-mat/0004205.
8. S. Tarucha et al.: Phys. Rev. Lett. **84**, 2485 (2000); D.G. Austing et al.: Phys. Rev. B **60**, 11514 (1999); L. P. Kouwenhoven et al.:, Science **278**, 1788 (1997)
9. M. Eto and Y. Nazarov: Phys. Rev. Lett. **85**, 1306 (2000)
10. M. Pustilnik and L. I. Glazman: Phys. Rev. Lett. **85**, 2993 (2000)
11. M. Pustilnik and L. I. Glazman: unpublished.
12. L. I. Glazman and M. E. Raikh: JETP Lett. **47**, 452 (1988); T. K. Ng and P. A. Lee: Phys. Rev. Lett. **61**, 1768 (1988)
13. T. Inoshita *et al.*: Phys. Rev. B **48**, 14725 (1993); L. I. Glazman, F. W. Hekking, and A. I. Larkin: Phys. Rev. Lett. **83**, 1830 (1999); A. Kaminski, L. I. Glazman: Phys. Rev. B **61**, 15297 (2000)
14. I. Affleck, A. W. W. Ludwig, and B. A. Jones: Phys. Rev. B **52**, 9528 (95); A. J. Millis, B. G. Kotliar, and B. A. Jones: In *Field Theories in Condensed Matter Physics*, ed. by Z. Tesanovic (Addison Wesley, Redwood City, CA, 1990), pp. 159-166
15. P. Nozières: J. Low Temp. Phys. **17**, 31 (1974)
16. P. W. Anderson: J. Phys. C **3**, 2436 (1970)
17. Y. Meir, N. S. Wingreen, and P. A. Lee: Phys. Rev. Lett. **70**, 2601 (1993); N. S. Wingreen and Y. Meir: Phys. Rev. B **49**, 11040 (1994)
18. A. Kaminski, Yu. V. Nazarov, and L. I. Glazman: Phys. Rev. Lett. **83**, 384 (1999); Phys. Rev. B **62**, 8154 (2000)
19. M. Pustilnik, Y. Avishai, and K. Kikoin: Phys. Rev. Lett. **84**, 1756 (2000)
20. I. E. Smolyarenko and N. S. Wingreen: Phys. Rev. B **60**, 9675 (1999)

21. A. M. Tsvelik and P. B. Wiegmann: Adv. Phys. **32**, 453 (1983)
22. T. A. Costi and A. C. Hewson, and V. Zlatić: J. Phys. CM **6**, 2519 (1994)
23. S. Sasaki et al.: Nature **405**, 764 (2000)
24. The top contact is obtained by deposition of Au/Ge and annealing at 400 $^{\circ}C$ for 30 s. This thermal treatment is gentle enough to prevent the formation of defects near the dot, but does not allow the complete suppression of the native Schottky barrier. The residual barrier leads to electronic confinement and corresponding charging effects in the GaAs pillar.
25. S. Tans et al.: Nature **386**, 474 (1997); C. Dekker, Physics Today **52**, 22 (1999)
26. S. Tans et al.: Nature **394**, 761 (1998)
27. M. Bockrath, et al.: Science **275**, 1922 (1997); M. Bockrath, et al.: Nature **397**, 598 (1999)
28. D. H. Cobden et al.: Phys. Rev. Lett. **81**, 681 (1998)
29. J. Nygård, D. H. Cobden, and P. E. Lindelof: Nature, *in press*
30. A. Thess et al.: Science **273**, 483 (1996)